

# Modeling Strategies for the Propagation of Terminal Double Bonds During the Polymerization of N-Vinylpyrrolidone and Experimental Validation

Christian Zander,\* Klaus-Dieter Hungenberg,\* Thomas Schall, Christian Schwede, and Ulrich Nicken

Based on a recently suggested reaction mechanism, which involves the production and propagation of terminal double bonds (TDBs), kinetic models for the polymerization of N-vinylpyrrolidone in aqueous solution are developed. Two modeling strategies, the classes and the pseudodistribution approach, are applied to handle the multidimensional property distributions that result from this reaction mechanism and to get detailed structural property information, e.g., on the chain length distribution and the distribution of TDBs. The structural property information is then used to develop reduced models with significantly lower computational effort, which can be used for process design, on-line applications or coupled to computational fluid dynamic simulations. To validate the derivations, the models are first compared against each other and finally to experimental results from a continuous stirred tank reactor. The evolution of monomer conversion and molecular weight average data as well as molecular weight distributions can be represented very well by the models that are derived in this article. These results support the correctness of the reaction mechanism predicted by quantum mechanical simulations.


## 1. Introduction

Specialty polymers such as polyvinylpyrrolidone (PVP) are mostly produced in batch or semibatch processes due to the need for flexibility for the production of this product class. In

C. Zander, T. Schall, Prof. U. Nicken  
Institut für Chemische Verfahrenstechnik  
Universität Stuttgart  
Böblinger Str. 78, Stuttgart 70199, Germany  
E-mail: icvt@icvt.uni-stuttgart.de

Prof. K.-D. Hungenberg  
Hungenberg Consultant  
Ortsstrasse 135  
Birkenau 69488, Germany  
E-mail: kdh.consult@yahoo.de

Dr. C. Schwede  
BASF SE  
Ludwigshafen 67056, Germany

 The ORCID identification number(s) for the author(s) of this article can be found under <https://doi.org/10.1002/mren.202000009>.

© 2020 The Authors. Published by WILEY-VCH Verlag GmbH & Co. KGaA, Weinheim. This is an open access article under the terms of the Creative Commons Attribution License, which permits use, distribution and reproduction in any medium, provided the original work is properly cited.

DOI: 10.1002/mren.202000009

the course of process intensification, new processes in continuous reactor systems are under investigation to improve process control and energy efficiency. One of the major problems in the development of processes in such reactor systems is occurrence of fouling. While the problem can be handled in tank reactors with a low volume-specific surface area, it may cause blocking and consequent shut down of tubular reactors with static mixer elements under certain operating conditions and prohibits the continuous operation of such reactor systems. If side reactions that produce high molecular weight and highly branched polymer chains are relevant in the reaction mechanism, local backmixing may enhance the formation of polymer networks that are insoluble and form a polymer gel. This may only be the case in some solvents or in certain ranges of the feed composition.<sup>[1–3]</sup> To predict process

windows in which operation is possible and to get information on the polymer microstructure, quantitative kinetic models that capture all relevant reactions are necessary.

Several publications on the reaction mechanism and kinetics of the polymerization of N-vinylpyrrolidone (NVP) in various solvents exist. The propagation rate coefficients in aqueous and organic solution<sup>[4,5]</sup> as well as the termination rate coefficient in aqueous solution<sup>[6]</sup> have been studied extensively using pulsed laser polymerization-size exclusion chromatography (PLP-SEC). While termination by combination seems to be the relevant mechanism in aqueous solution, transfer reactions to the solvent dominate the termination in organic solution.<sup>[7]</sup> Besides transfer to solvent molecules, transfer to monomer has also been proposed to take part in the reaction mechanism.<sup>[8]</sup> Some confusion exists about transfer mechanisms that are relevant for long chain branching during the polymerization in aqueous solution. Since broad, high molecular tails have been observed in the molecular weight distribution in batch and semibatch experiments, transfer to polymer has been assumed to be part of the reaction mechanism.<sup>[8]</sup> Recently, another mechanism has been suggested in which creation of terminal double bonds (TDBs) by transfer to monomer and subsequent propagation of TDBs is the reason for long chain branching.<sup>[9]</sup> The suggestion was motivated by

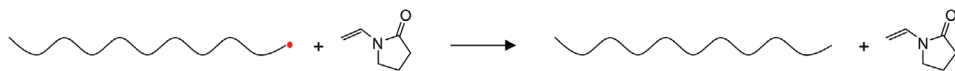


**Figure 1.** Reaction scheme of the transfer to monomer reaction. The radical center (red) is transferred to a monomer molecule by H-abstraction. Adapted and simplified from ref. [9].

calculations from density functional theory (DFT) and validated by batch experiments.

In this article, we revisit the aqueous phase polymerization of NVP in backmixed reactors. Our goal is to systematically develop kinetic models, which can be used to get detailed microstructural property information, e.g., on chain length or TDBs, but may also be applied in parameter estimations or CFD simulations in which the computational effort needs to be low. Since these objectives are contradictory, multiple models with different levels of detail need to be developed and the informational content must be transferred consistently between levels. For this purpose, we apply two modeling approaches, the classes<sup>[10,11]</sup> and the pseudodistribution approach,<sup>[10,12–14]</sup> to handle the multidimensional property distributions that result from the reaction mechanism described by Deglmann et al.<sup>[9]</sup> We condense the detailed information gained from simulations using these models and use it to develop much simpler models with significantly lower computational effort. To refine the kinetic coefficients from ref. [9] and to test the predictive capability of the models, we compare simulation results with experimental results for monomer conversion, molecular weight averages and molecular weight distributions from CSTR experiments.

This article is organized as follows. In Section 2, the reaction mechanism of the polymerization of NVP in aqueous solution as well as correlations for kinetic coefficients from literature are summarized briefly and the set of reactions that are the basis of the model development are defined. In Section 3, different modeling strategies for multidimensional property distributions are explained and applied to the reaction system from Section 2 and the simulations are compared to experimental results in Section 4. Finally, the results are concluded and a workflow for the application of the models that have been developed is suggested in Section 5. The experimental and numerical details are explained in Section 6.

## 2. Reaction Mechanism of the Polymerization of NVP

The reaction scheme we assume in this article was identified and discussed in detail in ref. [9]. Initiation, propagation of monomer M and termination are the main reactions in the radical polymerization of NVP in aqueous solution and lead to linear polymer chains. Only termination by combination has been assumed, since this is considered to be the

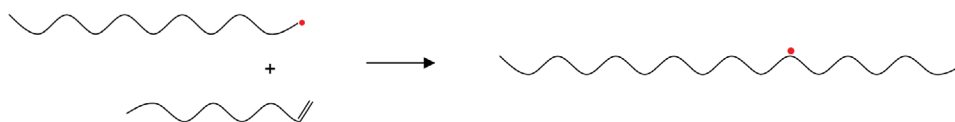


**Figure 2.** Terminal double bond (TDB) propagation reaction for a polymer chain carrying only one TDB. A mid chain radical is created and causes long chain branching. Adapted and simplified from ref. [9].

relevant termination mechanism for monosubstituted vinyl-monomers.<sup>[15]</sup> The two side reactions, transfer to monomer, which initiates a new polymer radical carrying a TDB as illustrated in **Figure 1** and the propagation of TDBs as illustrated in **Figure 2** may lead to branched or crosslinked polymer chains.

The system of interest is characterized by three property coordinates: the chain length  $n$ , the number of TDBs  $i$  and the number of branches  $k$ . It should be noticed, that the property dimensions  $i$  and  $k$  are linked—but not directly. TDBs are produced by transfer to monomer and consumed by the TDB propagation reaction. The number of branching points, on the other hand, increases only, if TDBs are consumed, not when they are produced.

Thus, the simulation of the evolution of a 3D property distribution would be necessary to describe the system in full detail. In principal, if reactions between polymer radicals carrying TDBs were included in the model, the number of radical centers per molecule would have to be considered as a fourth property coordinate. Since the complexity of the model would increase even further, we will not consider this here and restrict the model to species with either zero or one radical center as in ref. [9]. We refer to these as the dead species  $P$  and living species  $R$  respectively.

The full set of reactions that have been proposed to be relevant in the radical polymerization of NVP in aqueous solution in ref. [9] is shown in **Table 1** for the full 3D system. Since the rate of the TDB propagation reaction is proportional to the number of TDBs, the reaction scheme is nonlinear in the TDB property coordinate.

Most of the rate coefficients in Table 1 are taken from literature. The propagation rate coefficient can be calculated from ref. [4] according to

$$\frac{k_p}{k_{p,\max}} = 0.36 + 0.64 \exp(-9.2 w_{\text{NVP}}) - 0.31 w_{\text{NVP}} \quad (1)$$

with

$$k_{p,\max}/\text{L mol}^{-1} \text{ s}^{-1} = 2.57 \times 10^7 \exp\left(-\frac{17.6 \text{ kJ mol}^{-1}}{RT}\right) \quad (2)$$

and  $w_{\text{NVP}}$ , the weight fraction of NVP in the mixture. As in ref. [8], the transfer to monomer rate coefficient has been assumed to be proportional to the monomer propagation rate coefficient with a ratio of  $k_{t,m}/k_p = 6 \times 10^{-4}$ . The termination rate coefficient depends on the monomer weight fraction in



**Table 1.** Full set of reactions for the polymerization of NVP in aqueous solution (based on ref. [10]). The definition of rate coefficients and species is given in the text.

Initiation	$I_2 \xrightarrow{k_d} 2f_d I + M \xrightarrow{k_s} R_{1,0,0}$
Propagation	$R_{n,j,k} + M \xrightarrow{k_p} R_{n+1,j,k}$
Termination by combination	$R_{n,j,k} + R_{m,j,l} \xrightarrow{k_{tc}} P_{n+m,j+k+l}$
Transfer to monomer	$R_{n,j,k} + M \xrightarrow{k_{tm}} P_{n,j,k} + R_{1,1,0}$
Propagation of terminal double bonds	$R_{n,j,k} + P_{m,j,l} \xrightarrow{j \cdot k_{p,TDB}} R_{n+m,j+k+l+1}$

the low conversion regime in which segmental diffusion (SD) is the rate determining mechanism. With increasing polymer content, viscosity increases and translational diffusion (TD) limits the termination rate until at very high polymer contents reaction diffusion (RD) determines the termination rate. Based on these mechanisms, a correlation for the termination rate coefficient of the form

$$k_t / \text{L mol}^{-1} \text{ s}^{-1} = \left( \frac{1}{k_{SD}} + \frac{\eta}{k_{TD}} \right)^{-1} + k_{RD} \quad (3)$$

has been proposed<sup>[6]</sup> with the rate coefficients  $k_{SD}$ ,  $k_{TD}$ , and  $k_{RD}$  for each mechanism respectively and the relative bulk viscosity  $\eta$  that is related to the viscosity at zero conversion. The rate coefficients and a correlation for  $\eta$  at 40 °C and 2000 bar have been determined by single laser pulse experiments in combination with  $k_p$  data from literature to be<sup>[6]</sup>

$$k_{SD} / \text{L mol}^{-1} \text{ s}^{-1} = 4.87 \times 10^7 \exp\left(-\frac{W_{NVP}}{0.29}\right) + 5.67 \times 10^6 \quad (4)$$

$$k_{TD} = 31 k_{SD}, \quad \eta = \exp(14.75 w_{PVP}) \quad (5)$$

with the polymer weight fraction  $w_{PVP}$  in the mixture and

$$k_{RD} = 140 w_{NVP} k_p \quad (6)$$

The effect of pressure  $p$  on diffusion can be corrected by

$$k_{SD}(p) = k_{SD}(2000 \text{ bar}) \exp\left(-5.61 \times 10^{-4} \left(\frac{p}{\text{bar}} - 2000\right)\right) \quad (7)$$

Reaction diffusion does not play a significant role for the conditions under investigation in this article but has been implemented for completeness. The temperature dependence of the termination rate coefficient is usually low, and so, the correlation discussed above has been used without any correction as has been done in ref. [8].

For the decomposition rate coefficient of initiator  $I_2$  to the initiator radical species  $I$ , the correlation

$$k_d / \text{s}^{-1} = 9.17 \times 10^{14} \exp\left(-\frac{1.24 \times 10^2 \text{ kJ mol}^{-1}}{RT}\right) \quad (8)$$

**Table 2.** Parameters for the reference case. This setup has been used for all simulations, if not stated otherwise.

Kinetic coefficients		Equations (1) to (8)
$k_d, k_t, k_p$		$6 \times 10^{-4[8]}$
$k_{tm}/k_p$		2500
$k_{p,TDB} = 2500 \text{ L mol}^{-1} \text{ s}^{-1}$		0.7 <sup>[8]</sup>
$f_d$		
Feed		
Monomer weight fraction $w_{NVP}^0$		0.2
Initiator weight fraction $w_i^0$		0.0002
Solvent weight fraction $w_{H_2O}^0$		$1 - w_{NVP}^0 - w_i^0$
Feed rate $\dot{m}_F$ [g min <sup>-1</sup> ]		10.38
Initial conditions in reactor		
Solvent weight fraction $w_{H_2O}^0$		1
Reactor temperature $T_R$ [°C]		85
Reactor volume $V_R$ [mL]		650

taken from the supplier<sup>[8]</sup> has been used. The TDB propagation rate coefficient  $k_{p,TDB}$  as well as the initiator efficiency  $f_d$  have been estimated using experimental data.

### 3. Model Development

We use a reference case throughout the model development to test different models against each other. The reaction conditions and kinetic parameters are typical for the polymerization of NVP in aqueous solution in an isothermal CSTR and are summarized in Table 2. The average residence time

$$\tau = \frac{V_R \cdot \rho_{H_2O}}{\dot{m}_F} \quad (9)$$

with the reactor volume  $V_R$  and the mass feed rate  $\dot{m}_F$  is around 1 h. The pure component mass densities of the solvent and monomer at 85 °C have been assumed to be  $\rho_{H_2O} = 959 \text{ kg m}^{-3}$  and  $\rho_{NVP} = 989 \text{ kg m}^{-3}$  respectively.<sup>[8]</sup>

#### 3.1. Modeling Strategies for Multidimensional Property Distributions

Commercially available Galerkin-FEM solvers such as the one implemented in Predici are usually capable of solving problems with one discrete property dimension. Generally, an extension to more than one dimension would be possible, but the increased numerical effort makes this practically infeasible.<sup>[16]</sup> To simulate systems with multidimensional property distribution as described in Section 2, the problem has to be transformed into a series of 1D problems.

The straightforward way is to solve for one property dimension directly, e.g., the chain length, and define different populations—so-called classes—for the other discrete property dimensions,<sup>[11]</sup> e.g.,  $R_{n,1,0}$  for living polymer chains carrying one

TDB and zero branches,  $R_{n,2,1}$  for living polymer chains carrying two TDBs and one branch and so on for the present example. The reaction scheme can be derived by assigning numbers to the second and third property indices in Table 1, for example



Other properties, e.g., the number of radical centers per chain, may be used as well. As already mentioned, we do not consider polymer chains with multiple radical centers here, but the dead species  $P$  and living species  $R$  can be considered classes with one or zero radical centers, respectively. The advantage of the classes approach is that a multidimensional property distribution can be reconstructed from the concentration distributions of different classes. Since only a finite number of property classes can be considered, a cutoff class must be defined in which all classes for property indices that are higher than the cutoff value are collected. Reconsidering the example in Equation (10), a cutoff value of 10 for the number of TDBs and the number of branches would lead to



Of course, the computational effort increases with every additional property class, and so, this approach should only be used, if suitable cutoff values are not too high, typically lower than 10.<sup>[16]</sup>

If this is not the case, another approach using so-called pseudodistributions may be used.<sup>[13]</sup>

These pseudodistributions are defined as the moments on all discrete property coordinates except one—usually the chain length—that is solved for explicitly. For example

$$\sum_{k=0}^{\infty} k^o \sum_{i=0}^{\infty} i^l \frac{dP_{n,i,k}}{dt} = \Psi_n^{l,o} \quad (12)$$

is the  $l$ -th TDB and  $o$ -th branching moment for chains of length  $n$ . Taking the zeroth moments on all other property coordinates gives the distribution of chain lengths

$$\sum_{k=0}^{\infty} \sum_{i=0}^{\infty} \frac{dP_{n,i,k}}{dt} = \Psi_n^{0,0} = P_n \quad (13)$$

which is widely used in 1D models. The first moments of the other properties can be understood as chain length distributed counters for this property. For the system considered here,  $\Psi_n^{1,0}$  and  $\Psi_n^{0,1}$  give the concentration of TDBs and branches in chains of length  $n$  respectively. If the system is nonlinear in one of the property coordinates, a closure problem exists and an estimate for a higher moment of this property must be found by a suitable closure relation. In this case, using higher moments of this property is a necessity to minimize the effect of the closure relation on lower moments, while, otherwise, higher moments may be used to gain additional, averaged information.

As long as suitable closure relations can be found, moment models should be preferred, since a large number of classes, would have to be used for many applications.<sup>[10,16]</sup> For example, the number of TDBs may take very large values for some

**Table 3.** Set of the 2D reactions as basis of the model development.

Initiation	$I_2 \xrightarrow{k_i} 2f_{dl} / I + M \xrightarrow{k_p} R_{1,0}$
Propagation	$R_{n,j} + M \xrightarrow{k_p} R_{n+1,j}$
Termination by combination	$R_{n,j} + R_{m,j} \xrightarrow{k_{tc}} P_{n+m,j+j}$
Transfer to monomer	$R_{n,j} + M \xrightarrow{k_{tm}} P_{n,j} + R_{1,1}$
Propagation of terminal double bonds	$R_{n,j} + P_{m,j} \xrightarrow{j \cdot k_{p,TDB}} R_{n+m,j+j-1}$

process conditions in the present case. Therefore, we will either derive pseudodistribution models or adapt such models from literature for the polymerization of NVP. For validation purposes, a comparison to an equivalent model using property classes for the number of TDBs for the reference case will be made. A model with classes up to 10 TDBs is applicable in this case as will be seen in Section 3.3. We refer to this model as the TDB classes model.

The 3D balance equations that correspond to the reaction system in Table 1 are given in ref. [10] and will not be repeated here in full length. As an example, the contribution of the TDB propagation reaction is

$$\frac{dR_{n,i,k}}{dt} + = -k_{p,TDB} R_{n,i,k} \sum_{m=1}^{\infty} \sum_{j=0}^{\infty} \sum_{l=0}^{\infty} j P_{m,j,l} + k_{p,TDB} \sum_{m=1}^{n-1} \sum_{j=0}^{i+1} \sum_{l=0}^k j P_{m,j,l} R_{n-m,i-j+1,k+l-1} \quad (14)$$

and

$$\frac{dP_{n,i,k}}{dt} + = -k_{p,TDB} i P_{n,i,k} \sum_{m=1}^{\infty} \sum_{j=0}^{\infty} \sum_{l=0}^{\infty} R_{m,j,l} \quad (15)$$

for the living and the dead species respectively. Since the number of branches does not appear in any reaction rate and, therefore, has no direct feedback on the reaction kinetics, the property index may simply be dropped as long as no information on the distribution of branches is desired.<sup>[10]</sup> Therefore, we will use the 2D reaction system in Table 3 as the basis of the model development in this article. Since the chain length distribution is usually desired because it is experimentally accessible and determines the macroscopic properties of the product, we will start with the derivation of models that give the full chain length distribution in Section 3.2. As will be seen, closure relations are needed in these models due to the nonlinearity in the TDB propagation reaction. In Section 3.3, we will present a model that does not need any closure relation and, therefore, contains exactly the same averaged information as the original 2D model. Based on the model in Section 3.3, we will introduce a model with zero property dimensions, which can be applied in CFD simulations or parameter estimations, in Section 3.4. An overview of the kinetic models that are developed and used in this article is given in Table 4.

**Table 4.** Overview of all models used in this article.

Short name of model	Sections	Distributions	Definition
TDB classes	3.2, 3.3	$R_{n,i} = (0,1,\dots,i_{\max})$	Chain length ( $n$ ) distribution/class with $i$ TDBs of polymers with one radical center
		$P_{n,i} = (0,1,\dots,i_{\max})$	Chain length ( $n$ ) distribution/class with $i$ TDBs of polymers with no radical center
TDB moment	3.2	$\sum_{i=0}^{\infty} i^l R_{n,i} = \Phi_n^l$	$l$ -th TDB moment (pseudo) chain length ( $n$ ) distribution of polymers with one radical center
		$\sum_{i=0}^{\infty} i^l P_{n,i} = \Psi_n^l$	$l$ -th TDB moment (pseudo) chain length ( $n$ ) distribution of polymers with no radical center
TDB reduced moment	3.2.1	$\sum_{i=0}^{\infty} R_{n,i} = R_n$	Zeroth TDB moment chain length ( $n$ ) distribution of polymers with one radical center
		$\sum_{i=0}^{\infty} P_{n,i} = P_n$	Zeroth TDB moment chain length ( $n$ ) distribution of polymers with no radical center
TDB distribution	3.3	$\sum_{n=1}^{\infty} n^k R_{n,i} = \Lambda_i^k$	$k$ -th chain length moment (pseudo) TDB ( $i$ ) distribution of polymers with one radical center
		$\sum_{n=1}^{\infty} n^k P_{n,i} = M_i^k$	$k$ -th chain length moment (pseudo) TDB ( $i$ ) distribution of polymers with no radical center
TDB double moment	3.4	$\sum_{i=0}^{\infty} i^l \sum_{n=1}^{\infty} n^k R_{n,i} = \lambda^{k,l}$	$k$ -th chain length moment and $l$ -th TDB moment of polymers with one radical center
		$\sum_{i=0}^{\infty} i^l \sum_{n=1}^{\infty} n^k P_{n,i} = \mu^{k,l}$	$k$ -th chain length moment and $l$ -th TDB moment of polymers with no radical center

### 3.2. Chain Length as the Only Discrete Property Coordinate (TDB Moment Model)

If the full distribution of polymer chain lengths is of interest, which is mostly the case, a 1D model in the chain length property coordinate is desirable. The number of TDBs as a discrete property coordinate can be eliminated by applying the moment operator on this coordinate leading to the pseudodistributions

$$\sum_{i=0}^{\infty} i^l R_{n,i} = \Phi_n^l \quad (16)$$

for the  $l$ -th TDB moment of living polymer chains with  $n$  repeat units and

$$\sum_{i=0}^{\infty} i^l P_{n,i} = \Psi_n^l \quad (17)$$

as the equivalent for dead polymer chains. We have used the nomenclature as in ref. [10] for easier comparison. A detailed derivation of the model has been given in ref. [10] as well and we do not repeat it here but highlight only the most important properties.

As mentioned before, creation and propagation of TDBs are considered to be important side reactions, which may lead to broad chain length distributions and chains with very high molecular weights. The corresponding reaction rate is proportional to the number of TDBs incorporated in the chain that is involved in the propagation reaction and the set of equations of

the moments on  $i$  can, therefore, not be closed as illustrated for the zeroth TDB moments

$$\frac{\partial \Phi_n^0}{\partial t} + = -k_{p,\text{TDB}} \Phi_n^0 \sum_m \Psi_m^1 + k_{p,\text{TDB}} \sum_m \Psi_{n-m}^1 \Phi_m^0 \quad (18)$$

$$\frac{\partial \Psi_n^0}{\partial t} + = -k_{p,\text{TDB}} \Psi_n^1 \sum_m \Phi_m^0 \quad (19)$$

It has been shown that if equations up to the second TDB moment are solved, simple closure relations like

$$\Psi_n^3 = D' \frac{\Psi_n^2 \Psi_n^2}{\Psi_n^1} \quad (20)$$

for the third TDB moment are sufficient.<sup>[10]</sup>  $D'$  is a dispersity and is assumed to be constant for all chain lengths and all times. In this section we use  $D' = 1.15$ , which has been estimated using the steady state value

$$D' \approx \frac{\mu_{\text{classes}}^{0,3} \mu_{\text{classes}}^{0,1}}{\mu_{\text{classes}}^{0,2} \mu_{\text{classes}}^{0,2}} \quad (21)$$

with

$$\mu_{\text{classes}}^{0,1} = \sum_{i=0}^{i_{\max}} \sum_{n=1}^{\infty} i^l P_{n,i} \quad (22)$$

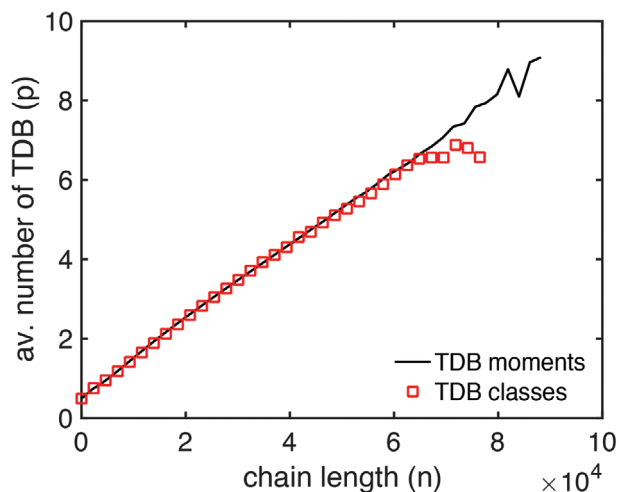


**Figure 3.** Comparison of the chain length averaged number of TDBs per molecule as a function of chain length for the TDB moment ( $D' = 1.15$ ) and classes models for the reference case.

of the TDB classes model for the reference case. Important information that can be extracted from the TDB moment model besides the chain length distribution are, for example, the average number of TDBs per chain of length  $n$

$$p(n) = \frac{\Psi_n^1}{\Psi_n^0} \quad (23)$$

as well as the corresponding ratio of the integrals over all chain lengths

$$\frac{\sum_n \Psi_n^1}{\sum_n \Psi_n^0} = \frac{c^{\text{TDB}}}{\lambda_0^p} \quad (24)$$

which is the average number of TDBs per molecule. As shown in **Figure 3**, the number of TDBs increases approximately linearly with the chain length starting at a value between 0 and 1 at  $n = 1$ . The chain length averaged number of TDBs per chain, which is illustrated in **Figure 4**, increases steeply in the beginning of the reaction and decreases at higher monomer conversion, which corresponds to higher polymer contents, when TDBs are consumed at a higher rate through the TDB propagation reaction. In **Figures 5** and **6**, the steady state chain length distribution and the evolution of monomer conversion are shown, and a comparison to the TDB classes model with classes for 0 up to a maximum of 10 TDBs per chain has been made, which demonstrates the validity of the implementation of both models and their applicability for the reference case. A discussion of the cutoff error of the TDB classes model is given in Section 3.3.

Although the computational effort for the TDB moment model is much lower in comparison to the TDB classes approach, it is still too high for extensive parameter studies and, therefore, further reduction of the model complexity is desirable.

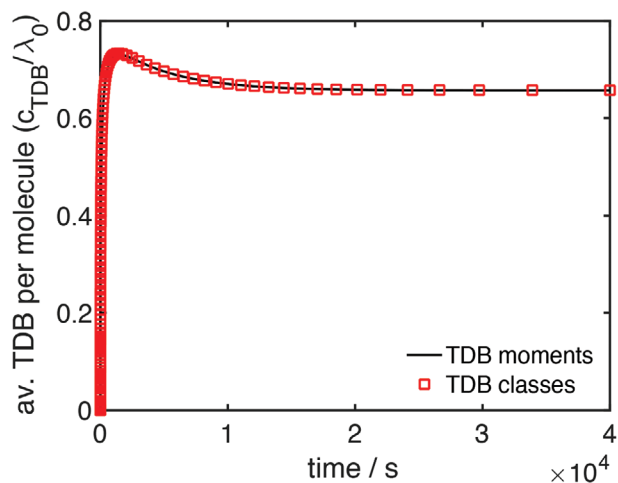


**Figure 4.** Comparison of the evolution of the average number of TDB per molecule for the TDB moment ( $D' = 1.15$ ) and classes models for the reference case.

### 3.2.1. Further Reduction of Model Complexity (TDB Reduced Moment Model)

The simplest possible model contains only two distributions—one for the living and one for the dead polymer species—as defined in Equation (13). As outlined in Section 3.2, closure relations are necessary if the moment approach is used on the number of TDB property coordinate because of the nonlinearity of the TDB propagation rate. For the case that only the evolution of the zeroth TDB moments  $\Psi_n^0$  and  $\Phi_n^0$  is calculated, an estimate for the first TDB moment  $\Psi_n^1$  is necessary. The contribution of the reaction rates for TDB propagation can be rewritten as

$$\begin{aligned} \frac{\partial \Phi_n^0}{\partial t} + &= -k_{p,\text{TDB}} \Phi_n^0 \sum_m \Psi_m^1 + k_{p,\text{TDB}} \sum_m \Psi_{n-m}^1 \Phi_m^0 = -k_{p,\text{TDB}} \Phi_n^0 \\ &\sum_m \frac{\Psi_m^1}{\Psi_m^0} \Psi_m^0 + k_{p,\text{TDB}} \sum_m \frac{\Psi_{n-m}^1}{\Psi_{n-m}^0} \Psi_{n-m}^0 \Phi_m^0 \end{aligned} \quad (25)$$

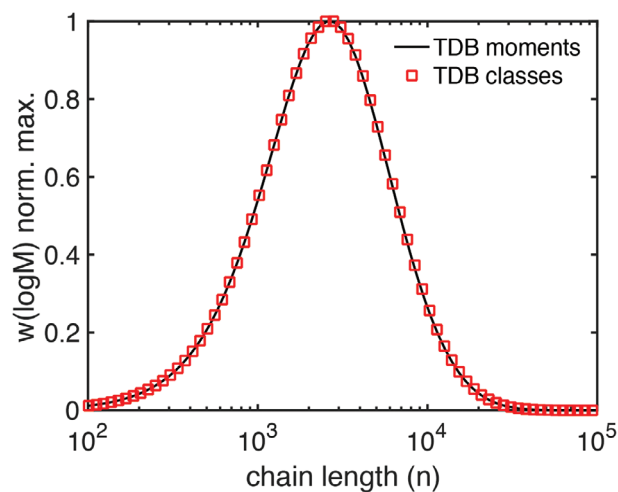


**Figure 5.** Comparison of the normalized GPC distribution for the TDB moment ( $D' = 1.15$ ) and classes models for the reference case.

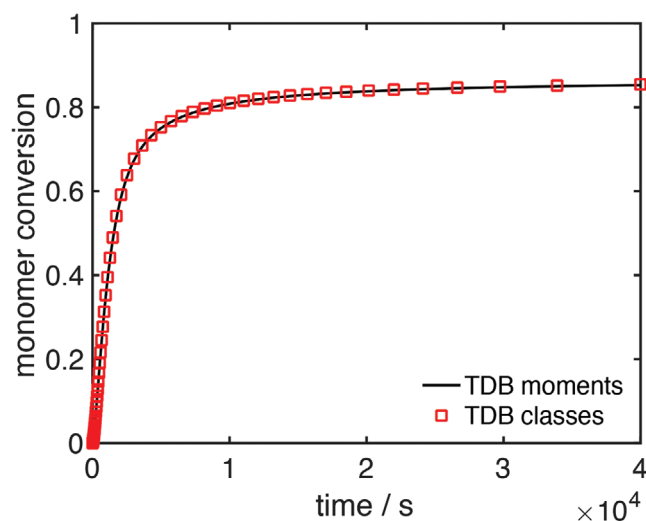


**Figure 6.** Comparison of the evolution of monomer conversion for the TDB moment ( $D' = 1.15$ ) and classes models for the reference case.

$$\frac{\partial \Psi_n^0}{\partial t} + = -k_{p,\text{TDB}} \Psi_n^1 \sum_m \Phi_m^0 = -k_{p,\text{TDB}} \frac{\Psi_n^1}{\Psi_n^0} \Psi_n^0 \sum_m \Phi_m^0 \quad (26)$$

which can be recast into the reaction scheme



The ratio  $\Psi_m^1/\Psi_m^0 = p(m)$  is the probability of finding a TDB in a dead chain of length  $m$ , which has been defined previously and can generally be calculated from higher moment models. As suggested by the results shown in Figure 3,  $p(n)$  may be approximated by two different linear relationships in  $n$

$$\frac{\Psi_n^1}{\Psi_n^0} \approx p_1(n) = A_1 \cdot n \quad (28)$$

$$\frac{\Psi_n^1}{\Psi_n^0} \approx p_2(n) = A_2 \cdot n + B_2 \quad (29)$$

The coefficient  $A_1$  can be determined by

$$c^{\text{TDB}} = \sum_{n=1}^{\infty} \Psi_n^1 = A_1 \sum_{n=1}^{\infty} n \cdot \Psi_n^0 = A_1 \cdot \lambda_1^p \quad (30)$$

and, therefore

$$p_1(n) = n \cdot \frac{c^{\text{TDB}}}{\lambda_1^p} \quad (31)$$

and for the second model with index 2 one of the coefficients may be determined by

$$c^{\text{TDB}} = \sum_{n=1}^{\infty} \Psi_n^1 = A_2 \sum_{n=1}^{\infty} n \cdot \Psi_n^0 + B_2 \sum_{n=1}^{\infty} \Psi_n^0 = A_2 \cdot \lambda_1^p + B_2 \cdot \lambda_0^p \quad (32)$$

If  $B_2$  is determined, then

$$p_2(n) = A_2 \cdot n + \frac{c^{\text{TDB}}}{\lambda_0^p} - A_2 \cdot \frac{\lambda_1^p}{\lambda_0^p} = A_2 \cdot (n - \overline{N}_n) + \frac{c^{\text{TDB}}}{\lambda_0^p} \quad (33)$$

with the number average chain length  $\overline{N}_n$  of dead polymer chains. The model including  $p_1(n)$  is actually equivalent to the model proposed in ref. [9] except that all dead and living species are collected in one distribution respectively. Similar approximations have also been suggested in refs. [17] and [18] for the TDB propagation rate in the polymerization of ethylene based on arguments using the reaction mechanism. The models described in refs. [9] and [17] include an estimate of  $c^{\text{TDB}}$  from a balance of a massless counter species<sup>[14]</sup>  $H^{\text{TDB}}$  that is produced and consumed with the same rates at which TDBs are produced or consumed. By introducing this counter species,  $c^{\text{TDB}}$  can be calculated without explicit knowledge of the distribution  $\Psi_n^1$  as

$$c^{\text{TDB}} = \sum_{n=1}^{\infty} \Psi_n^1 = H^{\text{TDB}} \quad (34)$$

For the sake of completeness, one can introduce an additional counter species  $H^B$  that allows the calculation of the average number of branches per molecule

$$n_0^B = \frac{H^B}{\lambda_0^p} \quad (35)$$

or per repeat unit

$$n_1^B = \frac{H^B}{\lambda_1^p} \quad (36)$$

However, we do not use this in the present article because a comparison with experimental data is not possible for the moment. The full set of reactions for this model, which we refer to as the TDB reduced moment model, including counter species is given in Table 5 using the common notation  $\Psi_n^0 = P_n$  and  $\Phi_n^0 = R_n$ .

The additional parameter  $A_2$  in Equation (33) may be fixed by extracting the slope of a linear fit to data from the TDB moment model presented in Figure 3. From Figure 7, it can easily be seen that  $p_2(n)$  gives a more realistic approximation of  $\Psi_n^1 = \Psi_n^0 \cdot p(n)$  than  $p_1(n)$ . While the approximation of  $\Psi_n^1$  that is calculated from simulations using  $p_2(n)$  is in reasonable agreement with

**Table 5.** Full set reactions for the TDB reduced moment model including counter species.

Initiation	$I_2 \xrightarrow{k_d} 2f_d \cdot I + M \xrightarrow{k_p} R_1$
Propagation of monomer	$R_n + M \xrightarrow{k_p} R_{n+1}$
Termination by recombination	$R_n + R_m \xrightarrow{k_{tc}} P_{n+m}$
Transfer to monomer	$R_n + M \xrightarrow{k_{tm}} P_n + R_1 + H^{\text{TDB}}$
Propagation of terminal double bonds	$R_n + P_m \xrightarrow{p(m) \cdot k_{p,\text{TDB}}} R_{n+m} + H^B - H^{\text{TDB}}$

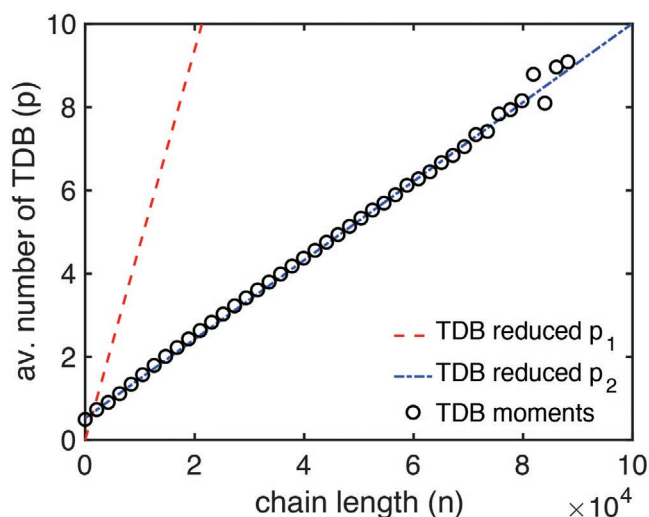


**Figure 7.** Comparison of the steady state chain length averaged number of TDBs per molecule as a function of chain length for the TDB moment ( $D' = 1.15$ ) and reduced models using  $p_1$  and  $p_2$  ( $A_2 = 9.49 \times 10^{-5}$ ) for the reference case.

the TDB moment model for the full range of chain lengths, applying  $p_1(n)$  results in a completely different form of the distribution. The reactivity of short chains is strongly underestimated, while that for long chains is overestimated.

In consequence,  $\bar{M}_w$  in **Figure 8** is in very good agreement with TDB moment model if  $p_2(n)$  is used, while it diverges if  $p_1(n)$  is applied.

Interestingly, the overall average concentration of TDBs per molecule in **Figure 9** as well as the number average molecular weight  $\bar{M}_n$  in **Figure 8** are in very good agreement with the TDB moment model for both approximations. The reason is that the coefficients of  $p_1(n)$  and  $p_2(n)$  have been fixed using the same integral value  $c^{\text{TDB}}$  in Equation (30) and Equation (32), and, therefore, the overall concentration of TDBs as well as the overall polymer concentration, e.g., the zeroth chain length moment, are the same for both approximations. Since the TDB propagation reaction does not influence the overall concentration of polymerized monomer units in chains  $R$  and  $P$ ,  $\bar{M}_n$  is not affected by the choice of  $p(n)$  either.

Since the approximation  $p_1(n)$  cannot represent the results from the TDB moment model adequately, we prefer  $p_2(n)$  although one more parameter needs to be fixed. The latter may be estimated from simulations using the TDB moment model as discussed in this section. We will revisit the estimation of the parameter  $A_2$  in Section 3.4.1.

### 3.3. Number of Terminal Double Bonds as the Only Discrete Property Coordinate (TDB Distribution Model)

The moment models introduced in Section 3.2 suffer from the drawback that the system of equations cannot be closed because the reaction mechanism is nonlinear in the discrete property coordinate  $i$ , the number of TDBs. The averaged information of these models can, therefore, not be exactly the same as that of the 2D original model, since additional assumptions in form

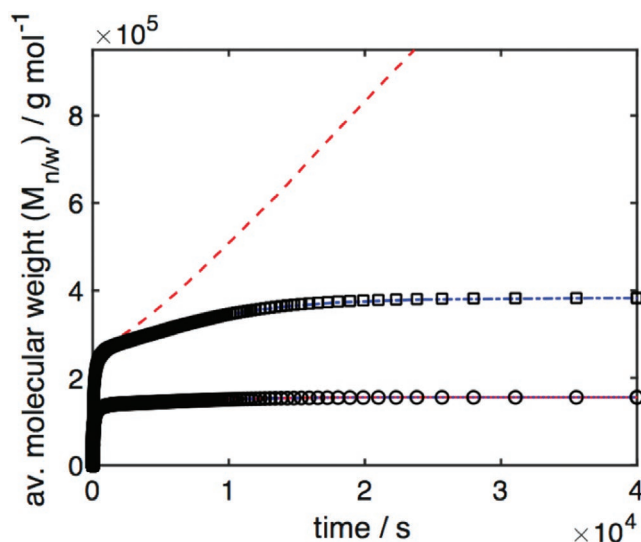


**Figure 8.** Comparison of the evolution of the molecular weight averages for the TDB moment ( $D' = 1.15$ ) and reduced models using  $p_1$  and  $p_2$  ( $A_2 = 9.49 \times 10^{-5}$ ) for the reference case: red solid—number average molecular weight  $\bar{M}_n$ , TDB reduced moment model using  $p_1$ ; blue dotted— $\bar{M}_n$ , TDB reduced moment model using  $p_2$ ; black circles— $\bar{M}_n$ , TDB moment model; red dashed—weight average molecular weight  $\bar{M}_w$ , TDB reduced moment model using  $p_1$ ; blue dashed-dotted— $\bar{M}_w$ , TDB reduced moment model using  $p_2$ ; black squares— $\bar{M}_w$ , TDB moment model.

of the closure relations Equation (20) and Equation (33) must be introduced. For the polymerization of NVP this problem can be circumvented by using the moment approach on the other discrete property coordinate, the chain length  $n$ , since no reaction rate is proportional to this property coordinate. The corresponding distributions are

$$\sum_{n=1}^{\infty} n^k R_{n,i} = \Lambda_i^k \quad (37)$$

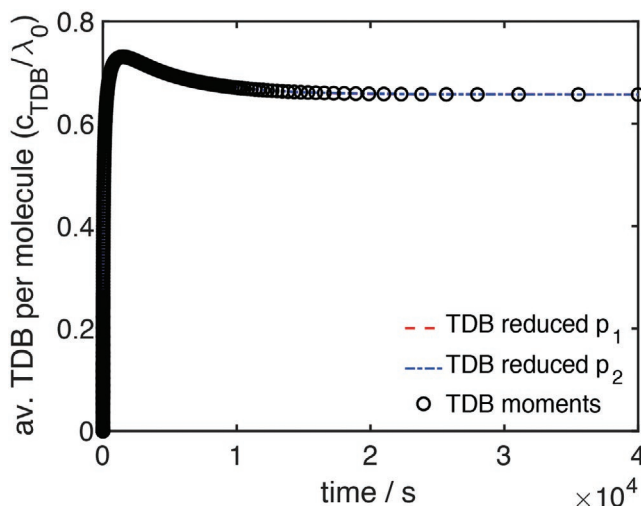


**Figure 9.** Comparison of the evolution of the average number of TDB per molecule for the TDB moment ( $D' = 1.15$ ) and reduced models using  $p_1$  and  $p_2$  ( $A_2 = 9.49 \times 10^{-5}$ ) for the reference case. Red and blue lines are indistinguishable by eye.



for the  $k$ -th chain length moment of living polymer chains carrying  $i$  TDBs and

$$\sum_{n=1}^{\infty} n^k P_{n,i} = M_i^k \quad (38)$$

as the equivalent for dead polymer chains. For the zeroth chain length moments  $\Lambda_i^0$  and  $M_i^0$ , the closed set of equations is

$$\frac{d\Lambda_i^0}{dt} = -k_{t,c}\Lambda_i^0 \sum_{j=0}^{\infty} \Lambda_j^0 - k_{tr,m}M\Lambda_i^0 - k_{p,TDB} \left( \Lambda_i^0 \sum_{j=0}^{\infty} jM_j^0 - \sum_{j=0}^{i+1} jM_j^0 \Lambda_{i-j+1}^0 \right) \quad (39)$$

$$\frac{dM_i^0}{dt} = \frac{1}{2}k_{i,c} \sum_{j=0}^i \Lambda_j^0 \Lambda_{i-j}^0 + k_{tr,m}M\Lambda_i^0 - k_{p,TDB}iM_i^0 \sum_{j=0}^{\infty} \Lambda_j^0 \quad (40)$$

Since this model gives the chain length averaged distribution of TDBs, we refer to it as the TDB distribution model. If only the chain length averaged distribution of TDBs is of interest, only the equations for the zeroth moments  $\Lambda_i^0$  and  $M_i^0$  need to be solved. Of course, higher moments offer additional information as for example the molecular weight averages

$$\overline{M}_n = \frac{\sum_{i=0}^{\infty} (\Lambda_i^1 + M_i^1)}{\sum_{i=0}^{\infty} (\Lambda_i^0 + M_i^0)} \cdot M_{\text{mono}} \quad (41)$$

$$\overline{M}_w = \frac{\sum_{i=0}^{\infty} (\Lambda_i^2 + M_i^2)}{\sum_{i=0}^{\infty} (\Lambda_i^1 + M_i^1)} \cdot M_{\text{mono}} \quad (42)$$

with the molecular weight of a repeat unit  $M_{\text{mono}}$ . The full set of equations of the TDB distribution model up to the second chain length moments  $\Lambda_i^2$  and  $M_i^2$  as well as a formulation in terms of reaction modules for the implementation in Predici are given in the Supporting Information. The average number of TDBs per chain defined in Equation (24) can be extracted as

$$\frac{c^{\text{TDB}}}{\lambda_0^p} = \frac{\sum_i iM_i^0}{\sum_i M_i^0} \quad (43)$$

but is not illustrated again. To demonstrate the information gained from this model, simulations using the reference case have been performed and compared to simulations using the TDB classes model to validate the derivation and implementation. In **Figure 10**, the concentration distribution as a function of TDBs is illustrated. With increasing number of TDBs, the concentration decreases rapidly by orders of magnitude. Despite their low concentration, these chains have a high reactivity because of the large number of incorporated TDBs. The relative difference between concentrations that are calculated from the TDB classes and the TDB distributions model is below 1% for polymers with up to 8 TDBs and increases to 3.5% and 29% for the polymers with 9 and 10 TDBs respectively. The estimates for the concentrations of chains with a large number of TDBs from the TDB classes model are higher,

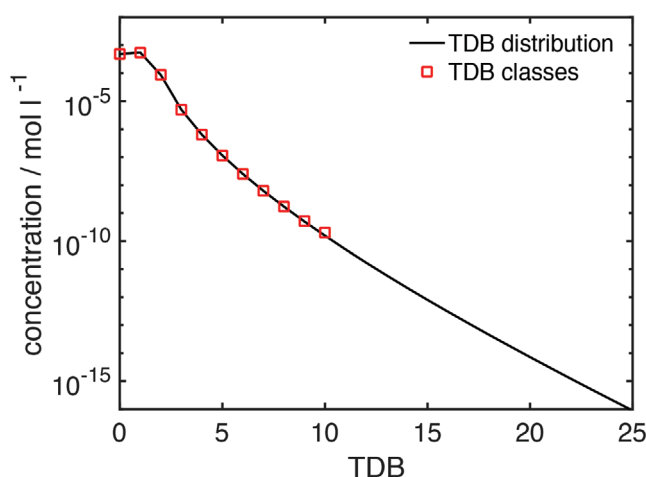


**Figure 10.** Comparison of the concentration distribution as a function of TDBs for the TDB distribution and classes models for the reference case.

since all molecules with 10 and more TDBs are collected in the cutoff distribution, which is the property class with 10 TDBs in this case. Nevertheless, a maximum of 10 TDBs per chain is a reasonable cutoff value for the reference case as is confirmed once more by the molecular weight averages that are shown in **Figure 11**.

Still, the classes model is computationally expensive. The TDB distribution model, on the other hand, can be applied for all process parameters that we have tested at a low computational cost, even in cases in which the concentration of polymers with more than 10 TDBs is relevant. It is, therefore, a more versatile benchmark and will be used as such subsequently.

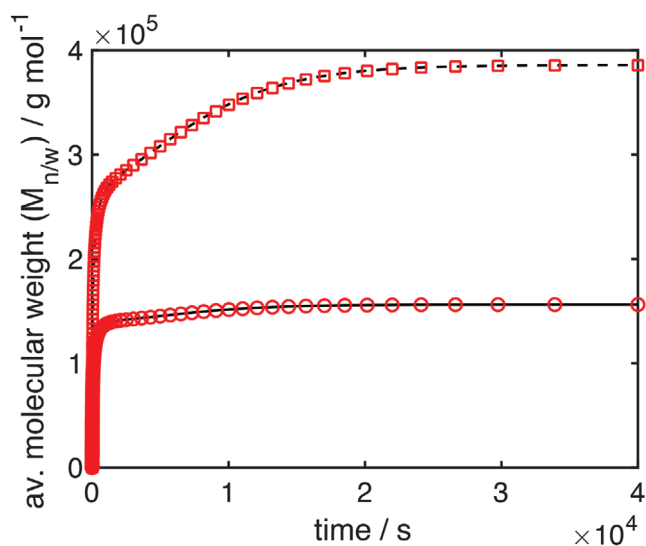


**Figure 11.** Comparison of the evolution of the molecular weight averages for the TDB distribution and classes models for the reference case: black solid—number average molecular weight  $\overline{M}_n$ , TDB classes model; red circles— $\overline{M}_n$ , TDB distribution model; black dashed—weight average molecular weight  $\overline{M}_w$ , TDB classes model; red squares— $\overline{M}_w$ , TDB distribution model.

### 3.4. A Moment Model on all Discrete Property Coordinates (TDB Double Moment Model)

For some applications, as for example the implementation in CFD codes or parameter estimations, models with zero property dimensions, e.g., moments taken on all property dimensions, are desirable because of the reduction of the computational effort. For the TDB reduced moment model, this is possible, but the redefined closure relation for the first TDB moment, Equation (33), introduces an additional parameter  $A_2$  into the model, which has to be estimated. The chain length moment version of the TDB reduced moment model is given in the Supporting Information for completeness, but we have not used it for any simulations in this article.

It is more desirable to derive a 0D model based on the TDB distribution model from Section 3.3, since no additional assumption has to be made in its derivation and the averaged information is exactly the same as that of the original 2D model. The quantities of interest are the double moments

$$\sum_{i=0}^{\infty} i^l \sum_{n=1}^{\infty} n^k R_{n,i} = \sum_{i=0}^{\infty} i^l \Lambda_i^k = \lambda^{k,l} \quad (44)$$

and

$$\sum_{i=0}^{\infty} i^l \sum_{n=1}^{\infty} n^k P_{n,i} = \sum_{i=0}^{\infty} i^l M_i^k = \mu^{k,l} \quad (45)$$

with the  $k$ -th moment on the chain length and the  $l$ -th moment on the number on TDBs  $\lambda^{k,l}$  and  $\mu^{k,l}$  for living and dead chains respectively. We refer to this model as the TDB double moment model. The resulting set of ODEs is quite lengthy, and the full model is given in the Supporting Information. As can be seen from

$$\begin{aligned} \frac{d\lambda^{2,2}}{dt} = & k_p M (2\lambda^{1,2} + \lambda^{0,2}) - k_{tc} \lambda^{2,2} \lambda^{0,0} - k_{tr,m} M (\lambda^{2,2} + \lambda^{0,0}) \\ & + k_{p,TDB} (2\lambda^{2,1} \mu^{0,2} - 2\lambda^{2,1} \mu^{0,1} + \lambda^{2,0} \mu^{0,3} - 2\lambda^{2,0} \mu^{0,2} \\ & + \lambda^{2,0} \mu^{0,1} + 2(\lambda^{1,2} \mu^{1,1} + 2\lambda^{1,1} \mu^{1,2} - 2\lambda^{1,1} \mu^{1,1} + \lambda^{1,0} \mu^{1,3} \\ & - 2\lambda^{1,0} \mu^{1,2} + \lambda^{1,0} \mu^{1,1}) + \lambda^{0,2} \mu^{2,1} + 2\lambda^{0,1} \mu^{2,2} - 2\lambda^{0,1} \mu^{2,1} \\ & + \lambda^{0,0} \mu^{2,3} - 2\lambda^{0,0} \mu^{2,2} + \lambda^{0,0} \mu^{2,1}) \end{aligned} \quad (46)$$

and

$$\begin{aligned} \frac{d\mu^{2,2}}{dt} = & k_{tc} (\lambda^{2,0} \lambda^{0,2} + 2\lambda^{2,1} \lambda^{0,1} + \lambda^{2,2} \lambda^{0,0} + \lambda^{1,0} \lambda^{1,2} + 2\lambda^{1,1} \lambda^{1,1} \\ & + \lambda^{1,2} \lambda^{1,0}) + k_{tr,m} M \lambda^{2,2} - k_{p,TDB} \lambda^{0,0} \mu^{2,3} \end{aligned} \quad (47)$$

closure relations are necessary due to the TDB propagation reaction. The moments  $\mu^{k,3}$  with  $k = 1, 2, 3$  are the chain length averaged moments

$$\mu^{k,3} = \sum_{i=0}^{\infty} i^3 M_i^k \quad (48)$$

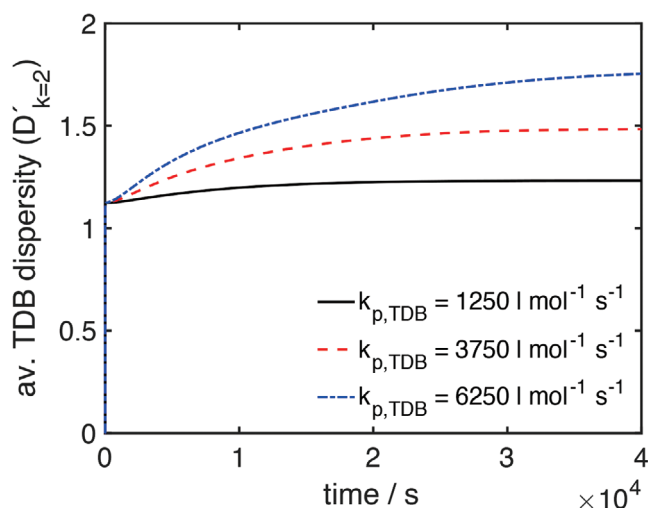


**Figure 12.** Effect of the variation of  $k_{p,TDB}$  on the evolution of the chain length averaged dispersity  $D'_{k=2}$  for the TDB distribution model for the reference case. The variation for  $k = 1, 2$  is even smaller.

which can generally be calculated from the TDB distribution model. It is convenient to define a chain length averaged closure relation similar to Equation (20) as

$$D'_k = \frac{\mu^{k,3} \mu^{k,1}}{\mu^{k,2} \mu^{k,2}} \quad (49)$$

and to specify  $D'_k$ . Three closure relations are needed in total, which does not sound very promising, but actually does not turn out to be a limitation for the system considered here. In **Figure 12** the dispersity defined in Equation (49) is shown for  $k = 2$  calculated from the TDB distribution model for a wide range of values for the TDB propagation rate coefficient  $k_{p,TDB}$ .  $D'_{k=2}$  varies only in a very narrow range between 1 and 2, and, therefore, a constant value of  $D'_k = 1$  for all  $k$  has been assumed, similar to that of Iedema et al.<sup>[10]</sup>

To verify this assumption, calculations with two different values for  $k_{p,TDB}$  have been carried out. The results of the TDB distribution model in **Figures 13** and **14** without any assumption and the TDB double moment model with  $D'_{k=\{0,1,2\}} = 1$  are in very good agreement. The reason for this observation is that the closure relations mostly influence the second TDB moments, while the zeroth TDB moments, which are needed for the calculation of the molecular weight averages from Equation (41) and Equation (42), are barely affected.

#### 3.4.1. Comparison to the TDB Reduced Moment Model

Finally, we make a comparison between the TDB double moment model and the TDB reduced moment model using the approximation  $p_2(n)$  to demonstrate an alternative way of fixing the parameter  $A_2$ . As can be seen from **Figure 15**, the results are generally in good agreement for the reference case but different values for the TDB propagation rate coefficient. The parameter  $A_2 = 9.49 \times 10^{-5}$  has been estimated from a

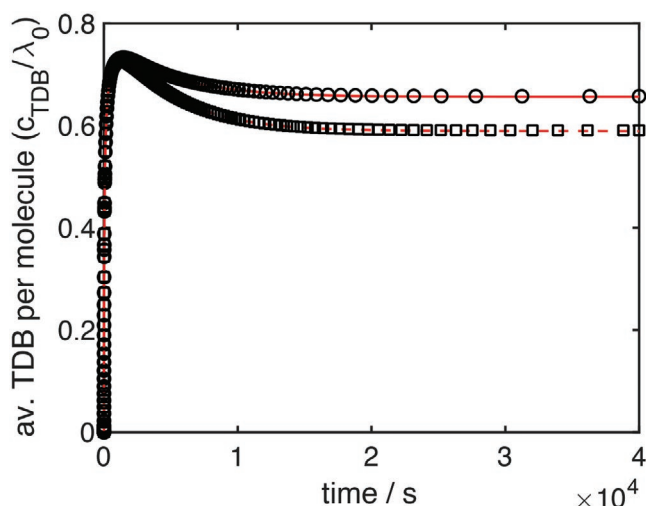


**Figure 13.** Comparison of the evolution of the average number of TDB per molecule for the TDB distribution and TDB double moment ( $D'_{k=\{0,1,2\}} = 1$ ) models for the reference case but different  $k_{p,\text{TDB}}$ : black circles—TDB distribution model,  $k_{p,\text{TDB}} = 2500$  L mol<sup>-1</sup> s<sup>-1</sup>; red solid—TDB double moment model,  $k_{p,\text{TDB}} = 2500$  L mol<sup>-1</sup> s<sup>-1</sup>; black squares—TDB distribution model,  $k_{p,\text{TDB}} = 6250$  L mol<sup>-1</sup> s<sup>-1</sup>; red dashed—TDB double moment model,  $k_{p,\text{TDB}} = 6250$  L mol<sup>-1</sup> s<sup>-1</sup>.

linear fit to data from a simulation of the reference case using the TDB moment model as illustrated in Figure 7. By comparison of the TDB propagation contribution to the evolution of the first chain length moment  $\lambda_1^p = \sum_n n P_n$  of the TDB reduced moment model

$$\frac{d\lambda_1^p}{dt} + = -k_{p,\text{TDB}}\lambda_0^R \left( A_2\lambda_2^p - A_2\frac{\lambda_1^p}{\lambda_0^p}\lambda_1^p + \frac{c^{\text{TDB}}}{\lambda_0^p}\lambda_1^p \right) \quad (50)$$

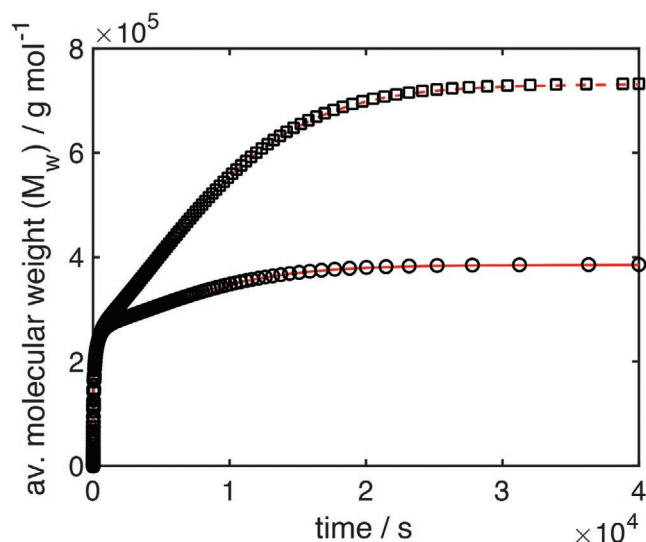


**Figure 14.** Comparison of the evolution of the weight average molecular weight  $M_w$  for the TDB distribution and TDB double moment ( $D'_{k=\{0,1,2\}} = 1$ ) models for the reference case but different  $k_{p,\text{TDB}}$ : black circles—TDB distribution model,  $k_{p,\text{TDB}} = 2500$  L mol<sup>-1</sup> s<sup>-1</sup>; red solid—TDB double moment model,  $k_{p,\text{TDB}} = 2500$  L mol<sup>-1</sup> s<sup>-1</sup>; black squares—TDB distribution model,  $k_{p,\text{TDB}} = 6250$  L mol<sup>-1</sup> s<sup>-1</sup>; red dashed—TDB double moment model,  $k_{p,\text{TDB}} = 6250$  L mol<sup>-1</sup> s<sup>-1</sup>.

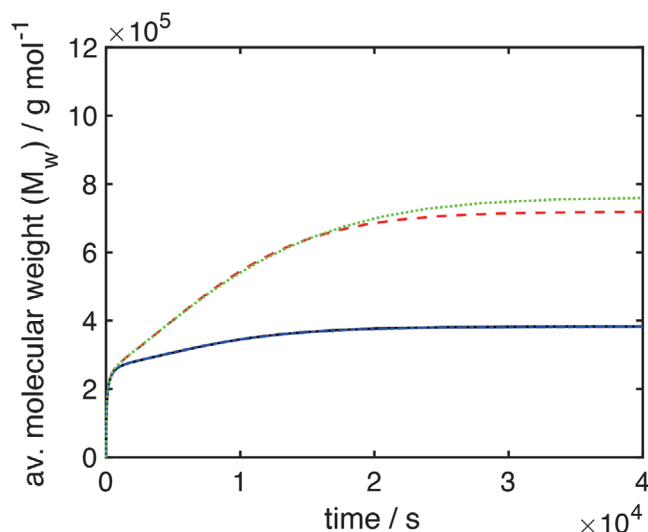


**Figure 15.** Comparison of the evolution of the weight average molecular weight  $M_w$  for the TDB reduced moment model with  $p_2$  ( $A_2 = 9.49 \times 10^{-5}$ ) and TDB double moment model ( $D'_{k=\{0,1,2\}} = 1$ ) for the parameters of the reference case but different  $k_{p,\text{TDB}}$ : black solid—TDB double moment model,  $k_{p,\text{TDB}} = 2500$  L mol<sup>-1</sup> s<sup>-1</sup>; blue dashed-dotted—TDB reduced moment model,  $k_{p,\text{TDB}} = 2500$  L mol<sup>-1</sup> s<sup>-1</sup>; red dashed—TDB double moment model,  $k_{p,\text{TDB}} = 6250$  L mol<sup>-1</sup> s<sup>-1</sup>; green dotted—TDB reduced moment model,  $k_{p,\text{TDB}} = 6250$  L mol<sup>-1</sup> s<sup>-1</sup>. The black and blue lines are indistinguishable by eye.

and the equivalent double moment  $\mu^{1,0} = \lambda_1^p$

$$\frac{d\mu^{1,0}}{dt} + = -k_{p,\text{TDB}}\lambda^{0,0}\mu^{1,1} \quad (51)$$

a definition of

$$A_2 = \frac{\mu^{1,1}\mu^{0,0} - \mu^{1,0}\mu^{0,1}}{\mu^{2,0}\mu^{0,0} - \mu^{1,0}\mu^{1,0}} \quad (52)$$

can be derived. Note, that  $c^{\text{TDB}} = \mu^{0,1}$ . For the reference case, the predicted steady state value  $A_2 = 9.48 \times 10^{-5}$  from the TDB double moment model computed with Equation (52) is very similar to the one that has been extracted from the TDB moment in Section 3.2.1.

For longer residence times with a steady state conversion of around 93%, the effect of  $k_{p,\text{TDB}}$  on  $A_2$  is more pronounced as shown in Figure 16. Figure 17 illustrates the influence of decreasing values of  $A_2$ , which are included in the TDB double moment model intrinsically, for different values of  $k_{p,\text{TDB}}$  on  $M_w$  at high residence times. The TDB reduced moment model using a fixed, constant value of  $A_2$  strongly overestimates the final  $M_w$  at higher values for  $k_{p,\text{TDB}}$ . Therefore, the assumption of a fixed value of  $A_2$  is only sufficient for conditions where the effect of TDB propagation is not too strong. As shown in Figure 18, using the calculated steady state value of the TDB double moment model from Equation (52) gives very good agreement of the steady state values of  $M_w$ , but the initial increase is underestimated, since the value of  $A_2$  decreases as TDBs are consumed. However, the influence is relatively low.

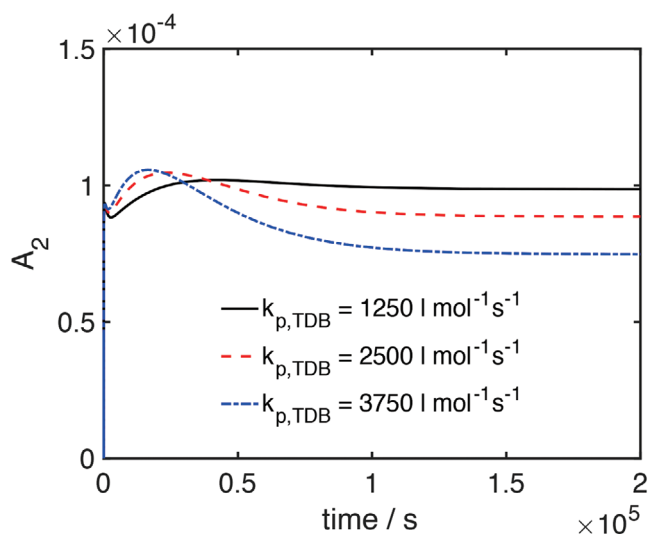


**Figure 16.** Comparison of the evolution of the parameter  $A_2$  calculated from the TDB double moment model ( $D'_{k=[0,1,2]} = 1$ ) for the parameters of the reference case with the residence time changed to 4.5 h and different values of the TDB propagation rate coefficient.

The value of  $A_2$  depends on the rate of consumption of TDBs but also on the rate of production of TDBs by the transfer to monomer reaction, especially on the ratio of the transfer to monomer to propagation rate. Since  $k_{tr,m}/k_p$  has been fixed in this article, we leave this study to the interested reader.

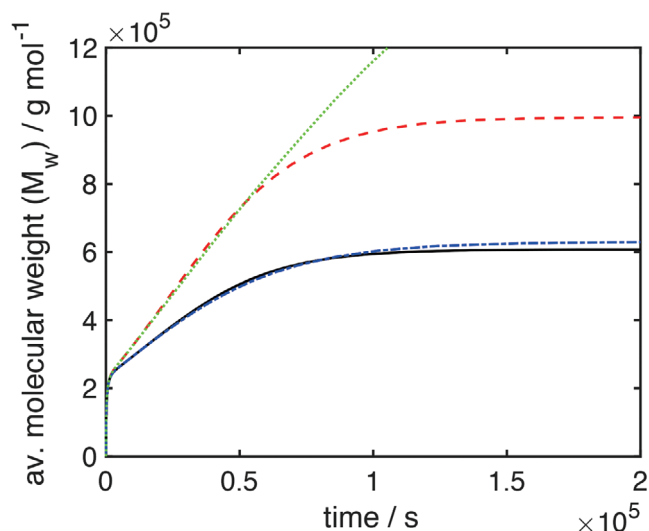


**Figure 17.** Comparison of the evolution of the weight average molecular weight  $\overline{M}_w$  for the TDB reduced moment model with  $p_2$  ( $A_2 = 9.49 \times 10^{-5}$ ) and TDB double moment model ( $D'_{k=[0,1,2]} = 1$ ) for the parameters of the reference case but average residence time changed to 4.5 h and different  $k_{p,TDB}$ : black solid—TDB double moment model,  $k_{p,TDB} = 2500$   $\text{L mol}^{-1} \text{s}^{-1}$ ; blue dashed-dotted—TDB reduced moment model,  $k_{p,TDB} = 2500$   $\text{L mol}^{-1} \text{s}^{-1}$ ; red dashed—TDB double moment model,  $k_{p,TDB} = 3750$   $\text{L mol}^{-1} \text{s}^{-1}$ ; green dotted—TDB reduced moment model,  $k_{p,TDB} = 3750$   $\text{L mol}^{-1} \text{s}^{-1}$ .

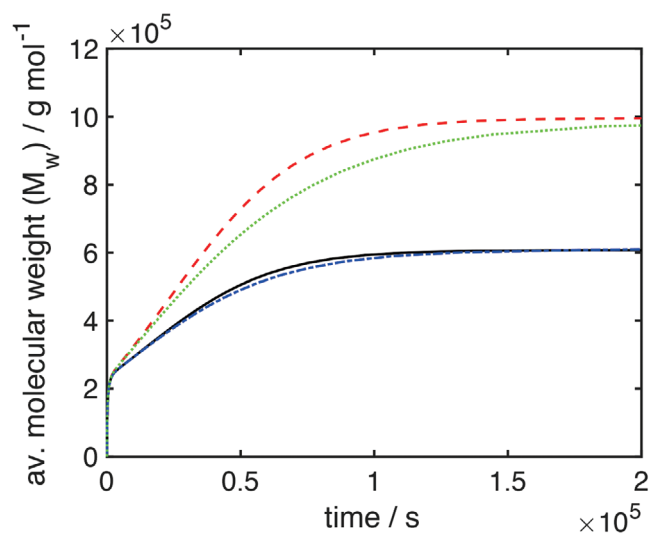


**Figure 18.** Comparison of the evolution of the weight average molecular weight  $\overline{M}_w$  for the TDB reduced moment model with  $p_2$  ( $A_2$  final value from Figure 16) and TDB double moment model ( $D'_{k=[0,1,2]} = 1$ ) for the parameters of the reference case but average residence time changed to 4.5 h and different  $k_{p,TDB}$ : black solid—TDB double moment model,  $k_{p,TDB} = 2500$   $\text{L mol}^{-1} \text{s}^{-1}$ ,  $A_2 = 8.85 \times 10^{-5}$ ; blue dashed-dotted—TDB reduced moment model,  $k_{p,TDB} = 2500$   $\text{L mol}^{-1} \text{s}^{-1}$ ,  $A_2 = 8.85 \times 10^{-5}$ ; red dashed—TDB double moment model,  $k_{p,TDB} = 3750$   $\text{L mol}^{-1} \text{s}^{-1}$ ,  $A_2 = 7.48 \times 10^{-5}$ ; green dotted—TDB reduced moment model,  $k_{p,TDB} = 3750$   $\text{L mol}^{-1} \text{s}^{-1}$ ,  $A_2 = 7.48 \times 10^{-5}$ .

## 4. Comparison to Experimental Results

The models in the preceding sections have been validated against each other using a reference case and capture the reaction mechanism correctly. To prove the applicability of the models to real life scenarios, we have performed experiments in a CSTR under conditions similar to the reference case. The process parameters are those of the reference case if not stated otherwise and are summarized in Table 6. We use  $\overline{M}_w$  data to estimate the rate coefficient of the TDB propagation reaction and make a comparison to molecular weight distributions subsequently.

### 4.1. Evolution of Molecular Weight Averages and Parameter Estimations

As specified in Table 6, experiments with different feed rates, e.g., residence times, have been carried out, and the results for  $\overline{M}_w$  and the monomer conversion are illustrated in Figures 19 and 20 respectively. The  $\overline{M}_w$  of samples that have been taken at different times during the experiment show an increase of  $\overline{M}_w$ , which depends strongly on the average residence time in the reactor.

Simulations using the TDB distribution model are in very good agreement with experimental data when using  $k_{p,TDB} = 3300$   $\text{L mol}^{-1} \text{s}^{-1}$  and all other kinetic parameters as specified in Table 2 except the initiator efficiency, which has been reduced to  $f_d = 0.6$  to match the monomer conversion. This value is slightly lower than the one used in ref. [9], which

**Table 6.** Parameters for comparison of simulations to experiments. The average residence time has been defined merely to identify the cases and rounded to quarter hours.

Kinetic coefficients	
$k_d, k_t, k_p$	Equations (1) to (8)
$k_{tr,m}/k_p$	$6 \times 10^{-4[8]}$
$k_{p,TDB}$ [L mol <sup>-1</sup> s <sup>-1</sup> ]	3300
$f_d$	0.6
Feed	
Monomer weight fraction $w_{NVP}^0$	0.2 or 0.1
Initiator weight fraction $w_i^0$	0.0002
Solvent weight fraction $w_{H_2O}^0$	$1 - w_{NVP}^0 - w_i^0$
Feed rate $\dot{m}_F$ [g min <sup>-1</sup> ]	14.16, 4.728, or 2.364
Initial conditions in reactor	
Solvent weight fraction $w_{H_2O}^0$	1
Reactor temperature $T_R$ [°C]	85
Reactor volume $V_R$ [mL]	650
Average residence time $\tau$ [h <sup>-1</sup> ]	$\approx 0.75, 2.25$ or 4.5

may be attributed to the steady state operation mode used in the present study. The TDB propagation rate coefficient is slightly higher than  $k_{p,TDB} = 2850$  L mol<sup>-1</sup> s<sup>-1</sup> that has been estimated in ref. [9] by comparison to experimental results. As discussed in Section 3.2.1, we attribute this to the different modeling approaches. The value of  $k_{p,TDB} = 3300$  L mol<sup>-1</sup> s<sup>-1</sup> that has been determined in this article is actually closer to the one predicted by DFT simulations, which is  $k_{p,TDB} = 4400$  L mol<sup>-1</sup> s<sup>-1</sup> for the same process parameters. However, the differences between

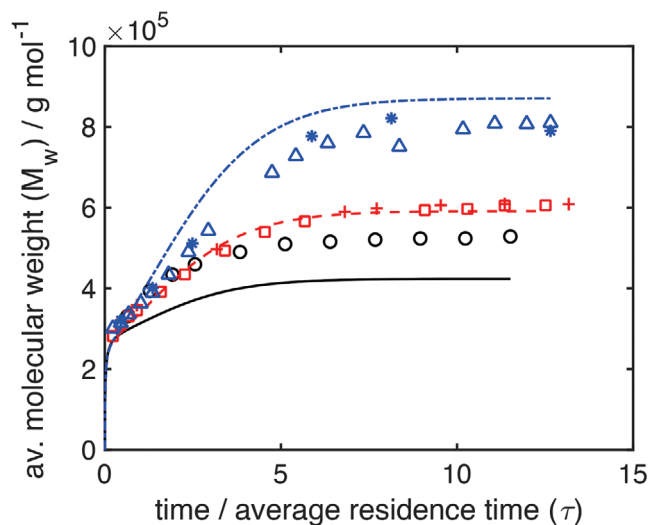


**Figure 19.** Comparison of the evolution of the weight average molecular weight  $M_w$  from experiments (markers) and simulations using the TDB distribution model (lines) for CSTR experiments with different average residence times: black circles, black solid line—0.75 h; red squares and crosses, red dashed line—2.25 h; blue triangles and stars, blue dashed dotted line—4.5 h. Different symbols denote repeated experiments.

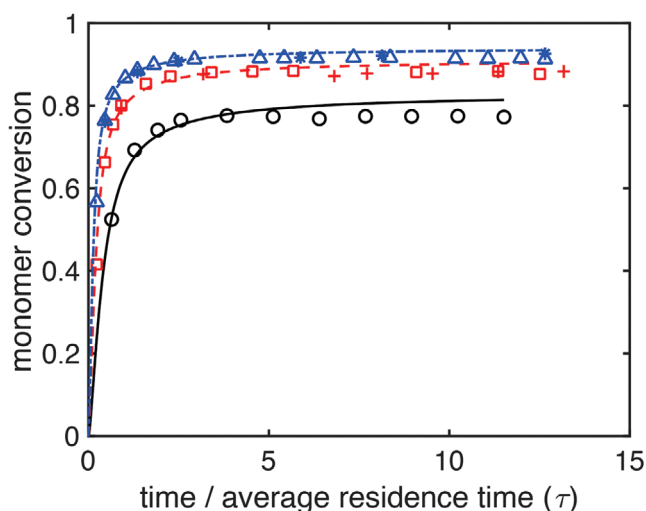


**Figure 20.** Comparison of the evolution of the monomer conversion from experiments (markers) and simulations using the TDB distribution model (lines) for CSTR experiments with different average residence times: black circles, black solid line—0.75 h; red squares and crosses, red dashed line—2.25 h; blue triangles and stars, blue dashed dotted line—4.5 h. Different symbols denote repeated experiments.

these three estimates of  $k_{p,TDB}$  are not large, which supports the correctness of the reaction mechanism predicted by quantum mechanical simulations in ref. [9] once more.

Since the TDB distribution model has a closed set of equations, no additional parameter or closure relation has to be specified. For computational reasons the parameters have been estimated using the TDB double moment model and the dispersities  $D'_{k=\{0,1,2\}} = 1$ , but the results of both models are indistinguishable as discussed in Section 3.4. Additionally, an experiment with a different monomer weight fraction has been carried out. The predicted values for  $\bar{M}_w$  and monomer conversion are also in very good agreement with simulated values as shown in Figures 21 and 22.

All of the experimental conditions that have been discussed in this section lead to steady state monomer conversion and molecular weight distributions. No gelation of the bulk phase occurred, which is in agreement with simulation results. As shown in Figures 23 and 24, simulations using the TDB double moment model predict gelation only for very high average residence times, which cannot be validated using the experimental equipment that we have employed for this article. Nevertheless, we have observed fouling deposits at the baffles of the tank reactor and in other poorly mixed regions which emphasizes the importance of dead water zones and diffusion on the formation of fouling deposits.

#### 4.2. Broadening of Molecular Weight Distributions and Comparison to the TDB Reduced Moment Model

The experimental molecular weight averages presented in Section 4.1 are in very good agreement with simulations using the TDB distribution or the TDB double moment model. Since the full chain length distributions are often of interest, a comparison of experimental distributions to simulations using the

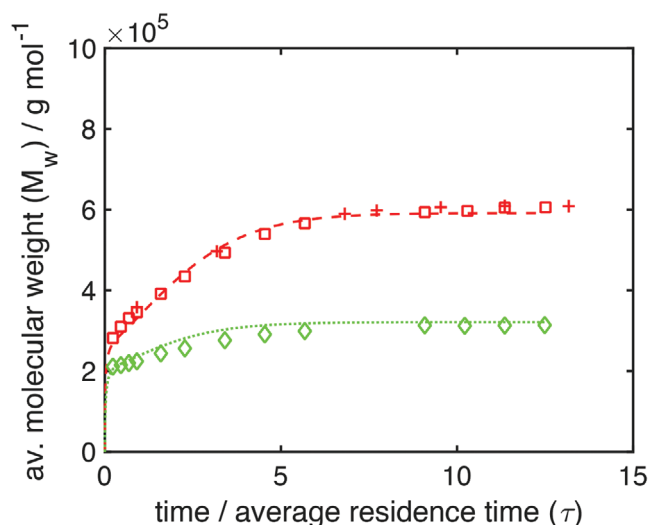


**Figure 21.** Comparison of the evolution of the weight average molecular weight  $\overline{M}_w$  from experiments (markers) and simulations using the TDB distribution model (lines) for CSTR experiments with different monomer weight fractions in the feed: red squares and crosses, red dashed line—20 wt% green diamonds, green dotted line—10 wt%. Different symbols denote repeated experiments.

TDB reduced moment model has been made. The parameter  $A_2$  has been chosen to be steady state value of the simulations using the TDB double moment model, which has been calculated from Equation (52). The simulation results for  $\overline{M}_w$  also match the experimental data very well as shown in Figure 25. Some differences to the results of the TDB distribution model exist and are attributed to the assumption of a constant value for parameter  $A_2$  as discussed in Section 3.4.1. A comparison of the full molecular weight distribution for the steady state GPC

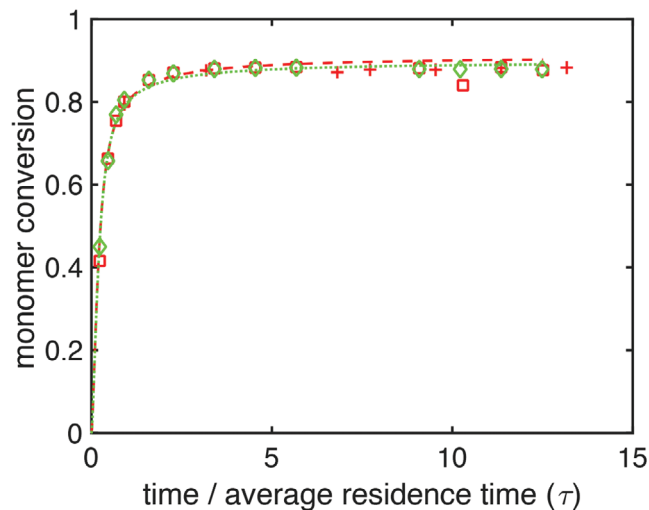


**Figure 22.** Comparison of the evolution of the monomer conversion from experiments (markers) and simulations using the TDB distribution model (lines) for CSTR experiments with different monomer weight fractions in the feed: red squares and crosses, red dashed line—20 wt%; green diamonds, green dotted line—10 wt%. Different symbols denote repeated experiments.

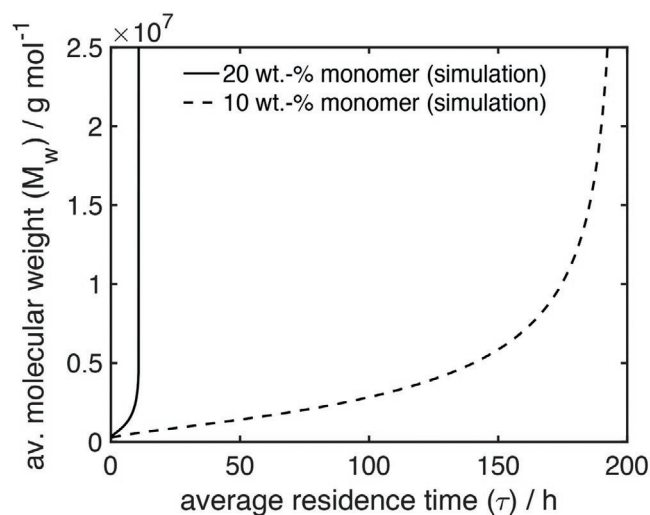


**Figure 23.** Dependence of the steady state weight average molecular weights  $\overline{M}_w$  from simulations using the TDB double moment model on the average residence time (Equation 9) for different monomer weight fractions in the feed.

distributions is shown in Figures 26–29 and shows very good agreement with the experimental results. The steady state  $\overline{M}_w$  data from experiments and model predictions that have been discussed in this section are listed in Table 7, and the steady state monomer conversion is listed in Table 8.

As can be seen in Table 7, the steady state  $\overline{M}_w$  is underestimated for low residence times and overestimated for high residence times. We do not have a definite explanation for this observation. The propagation of TDB is a reaction between two macromolecules and might be diffusion-limited like the termination reaction, for example. We assumed  $k_{p,TDB}$  to be constant, which would not be strictly correct in this case. It is possible,

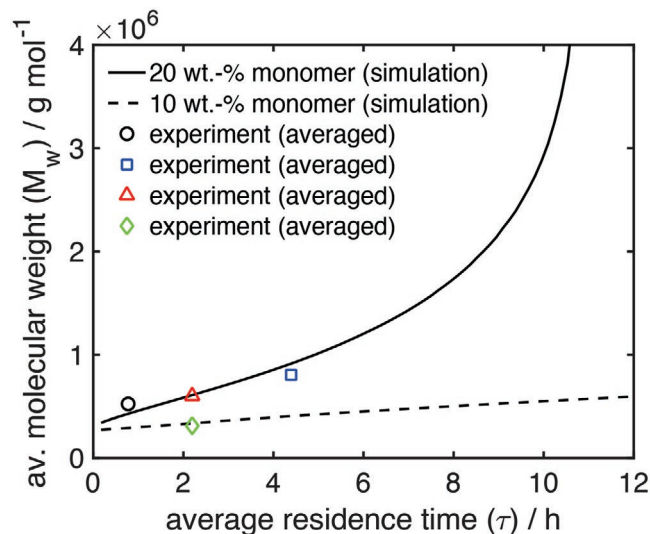


**Figure 24.** Magnification of Figure 23 and comparison to experiments for different average residence times (Equation 9) and monomer weight fractions in the feed. The experimental values are averaged steady state values of the experiments from Section 4.

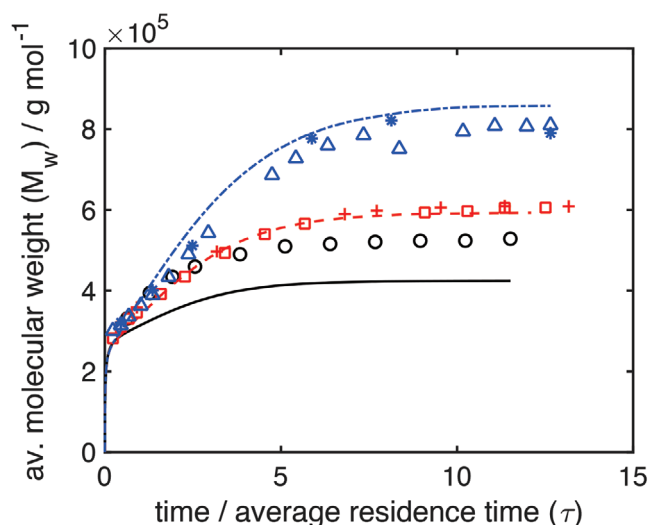


**Figure 25.** Comparison of the evolution of the weight average molecular weight  $M_w$  from experiments (markers) and simulations using the TDB reduced moment model (lines) with  $p_2$  for CSTR experiments with different average residence times: black squares, black solid line—0.75 h ( $A_2 = 9.3 \times 10^{-5}$ ); red squares and crosses, red dashed line—2.25 h ( $A_2 = 9.05 \times 10^{-5}$ ); blue triangles and stars, blue dashed dotted line—4.5 h ( $A_2 = 8.1 \times 10^{-5}$ ). Different symbols denote repeated experiments.

that the coefficient decreases with higher polymer content and, consequently, higher viscosity.

## 5. Conclusion

We have applied different modeling strategies to handle the multidimensional property distributions that result from the reaction mechanism of the polymerization of NVP in aqueous

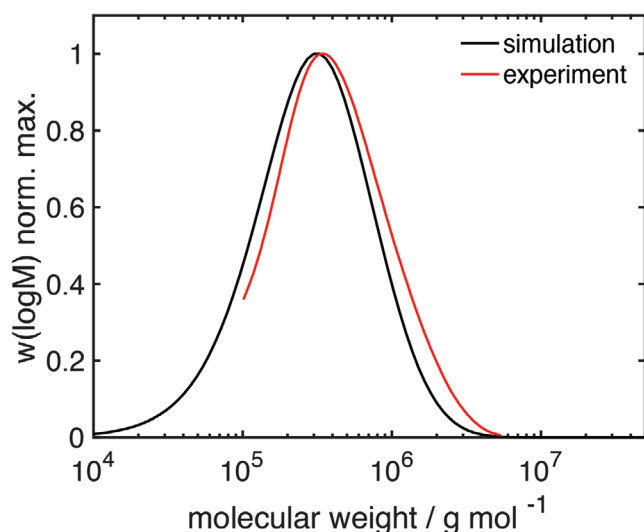


**Figure 26.** Comparison of the steady state normalized GPC distribution from experiment and simulation using the TDB reduced moment model with  $p_2$  ( $A_2 = 9.3 \times 10^{-5}$ ) for a CSTR experiments with an average residence time of 0.75 h and a monomer weight fraction of 20 wt% in the feed.

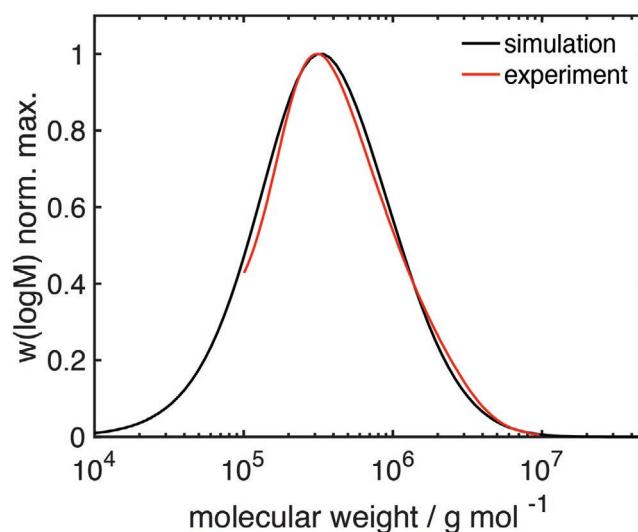


**Figure 27.** Comparison of the steady state normalized GPC distribution from experiment and simulation using the TDB reduced moment model with  $p_2$  ( $A_2 = 9.05 \times 10^{-5}$ ) for a CSTR experiments with an average residence time of 2.25 h and a monomer weight fraction of 20 wt% in the feed.

solution and compared the model predictions to experimental results from a CSTR.

The TDB classes model offers the most detailed information, and it is possible to reconstruct a 2D distribution from simulations using this model. The downside is the very high computational effort that restricts the application of this model to validation purposes under mild reaction conditions. The TDB moment model derived in ref. [10] reduces the computational effort and may be applied over a wider range of parameters, but, still, the numerical effort is too high for process design or

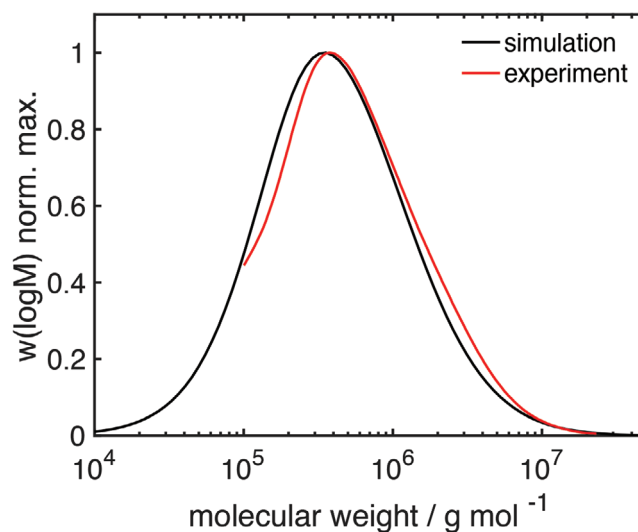


**Figure 28.** Comparison of the steady state normalized GPC distribution from experiment and simulation using the TDB reduced moment model with  $p_2$  ( $A_2 = 8.1 \times 10^{-5}$ ) for a CSTR experiments with an average residence time of 4.5 h and a monomer weight fraction of 20 wt% in the feed.

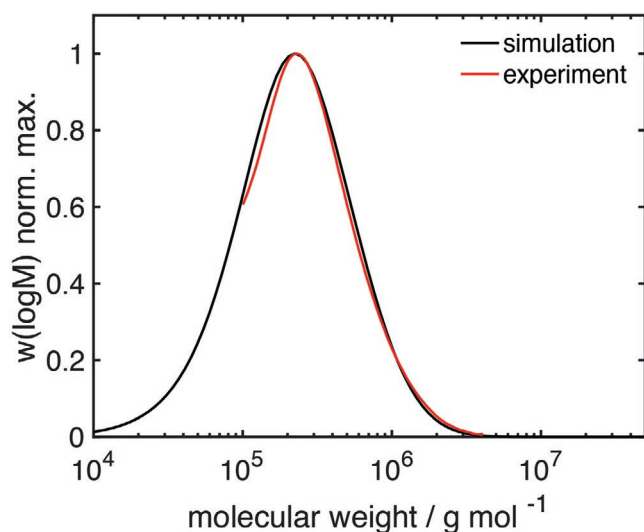


**Figure 29.** Comparison of the steady state normalized GPC distribution from experiment and simulation using the TDB reduced moment model with  $p_2$  ( $A_2 = 9.69 \times 10^{-5}$ ) for a CSTR experiments with an average residence time of 2.25 h and a monomer weight fraction of 10 wt% in the feed.

parameter estimations. Therefore, if the full molecular weight distribution is required, we recommend the TDB reduced moment model derived in Section 3.2, although the additional parameter  $A_2$  needs to be introduced. The TDB distribution model, which has been introduced in Section 3.3, offers averaged information without any additional parameter or closure relations and, therefore, gives exactly the same averaged results as the original 2D model. The computational effort can be reduced further by using the TDB double moment model from Section 3.4, which requires closure relations, but is not affected by their choice significantly. As discussed in Section 3.4.1, the parameter  $A_2$ , which is required for the TDB reduced moment model can be calculated from this model as well. The value does not remain constant but using the steady state value gives reasonable agreement of the steady state molecular weight averages and molecular weight distributions in CSTR experiments. Thus, we suggest to fix all rate coefficients using the TDB distribution or TDB double moment model and to estimate  $A_2$  for the TDB reduced moment model subsequently from these models if the full molecular weight distribution is desired.

**Table 7.** Comparison of steady state weight average molecular  $\overline{M}_w$  weight data from experiments and model predictions. The parameters are listed in Table 6.

Average residence time [h]	Monomer weight fraction in feed	Steady state $\overline{M}_w$ [ $10^3$ g mol $^{-1}$ ]		
		TDB distribution model	TDB reduced moment model	Experiment
0.75	0.2	424	424	524
2.25	0.2	591	592	601
4.5	0.2	870	857	805
2.25	0.1	321	318	313

**Table 8.** Comparison of steady state monomer conversion data from experiments and model predictions. Model predictions are the same for all models. The steady state values from simulations are all slightly higher than the experimental values, but the early stage monomer conversion can be captured best using the parameters listed in Table 6.

Average residence time [h]	Monomer weight fraction in feed	Steady state monomer conversion	
		Models	Experiment
0.75	0.2	0.81	0.77
2.25	0.2	0.9	0.88
4.5	0.2	0.93	0.91
2.25	0.1	0.89	0.88

The evolution of monomer conversion and molecular weight average data as well as molecular weight distributions can be represented very well using all of the developed models and the estimated value of the TDB propagation rate coefficient  $k_{p,TDB} = 3300$  L mol $^{-1}$  s $^{-1}$  is similar to the one that has been estimated in ref. [9] from batch experiments. These results support the correctness of the reaction mechanism predicted by quantum mechanical simulations in ref. [9] once more.

No gelation of the bulk phase occurred under the experimental conditions that have been used for this article, but we have observed fouling deposits in poorly mixed regions of the reactor. The effect of dead zones and diffusive mass transport on the formation of fouling deposits will be the focus of future work.

## 6. Experimental and Numerical Details

The experimental setups described in ref. [9] have been adapted for the purposes of this article.

**Chemicals:** N-vinylpyrrolidone stabilized with 0.5% NaOH was supplied by BASF SE and distilled under vacuum to remove stabilizer and high-molecular components directly before the experiments. Initiator (V-50, Wako Chemicals) was stored in the refrigerator and used as delivered. Deionized water has been used as solvent.

**Experiments:** CSTR experiments were performed isothermally using a Juchheim stainless steel stirred tank reactor with 650 mL internal volume. Two storage containers were prepared, one containing a mixture of monomer and solvent, the other one containing initiator dissolved in the solvent. Both storage containers were degassed under vacuum and the gaseous atmosphere was flushed with a small flow of argon throughout the experiment to prevent oxygen from entering. The feed streams were realized by two Knauer Smartline 1050 piston pumps with 10 mL pump heads and the mass flow rate was controlled using Bronckhorst mini CORI-FLOW mass flow meters and a PI controller. The feed streams from both storage containers were mixed in a static mixing tee with 0.5 mm thru-holes and a 10  $\mu$ m frit in the center port in a 1:1 ratio at ambient temperature before entering the reactor. Prior to the experiment, the reactor was filled with degassed solvent and heated to the desired temperature. To ensure the correct feed rate, a purge valve was installed right before the reactor and the feed streams were pumped into a separate waste container for some time. The experiments were run for around 12 average residence times to safely reach a steady state.

**Analytical Setups:** Monomer conversion was measured using HPLC with a mixture of water and acetonitrile (90:10) as eluent at 0.5 mL min $^{-1}$  and the UV adsorption was measured at 235 nm. Molecular weight averages and distributions were measured using GPC with DMAc + 5 g L $^{-1}$  LiBr as eluent at 0.8 mL min $^{-1}$ . A column set containing one



column with 100 Å and two 10 000 Å pore size (PSS GRAM combination ultrahigh columns set) was used for separation. A combination of a refractive index detector (Agilent 1260 Infinity II series) and a multiangle light scattering detector (PSS SLD7100) was used to obtain absolute molecular weight averages and distributions and data was recorded using the WinGPC software. The weight average molecular weight  $M_w$  was calculated from the detector data directly and a linear approximation of the measured calibration curve was used to obtain molecular weight distributions. For the latter, only molecular weights higher than 100 kg mol<sup>-1</sup> were considered.

*Simulations:* The models presented in this article were implemented in the commercially available software package Predici.

## Supporting Information

Supporting Information is available from the Wiley Online Library or from the author.

## Acknowledgements

The financial support of the German Federal Ministry for Economic Affairs and Energy (BMWi) under grant number 03EN2004F (KoPPonA 2.0) is gratefully acknowledged. The authors thank Dr. M. Wulkow from CIT GmbH for his support with the implementation in Predici.

## Conflict of Interest

The authors declare no conflict of interest.

## Keywords

kinetic modeling, propagation of terminal double bonds, pseudodistributions, radical polymerization, side reactions

Received: February 24, 2020

Revised: March 31, 2020

Published online: May 17, 2020

- [1] D. Kohlmann, M.-C. Chevrel, S. Hoppe, D. Meimaroglou, D. Chapron, P. Bourson, C. Schwede, W. Loth, A. Stammer, J. O. Wilson, P. Ferlin, F. Laurent, S. Engell, A. Durand, *Macromol. React. Eng.* **2016**, *10*, 339.
- [2] J. Urrutia, A. Peña, J. M. Asua, *Macromol. React. Eng.* **2017**, *11*, 1.
- [3] C. Bernstein, Dissertation, *Universität Hamburg* **2017**.
- [4] M. Stach, I. Lacić, D. Chorvat, M. Buback, P. Hesse, R. A. Hutchinson, L. Tang, *Macromolecules* **2008**, *41*, 5174.
- [5] L. Uhelská, D. Chorvát, R. A. Hutchinson, S. Santanakrishnan, M. Buback, I. Lacić, *Macromol. Chem. Phys.* **2014**, *215*, 2327.
- [6] J. Schrooten, M. Buback, P. Hesse, R. A. Hutchinson, I. Lacić, *Macromol. Chem. Phys.* **2011**, *212*, 1400.
- [7] F. Haaf, A. Sanner, F. Straub, *Polym. J.* **1985**, *17*, 143.
- [8] S. Santanakrishnan, L. Tang, R. A. Hutchinson, M. Stach, I. Lacić, J. Schrooten, P. Hesse, M. Buback, *Macromol. React. Eng.* **2010**, *4*, 499.
- [9] P. Deglmann, M. Hellmund, K. Hungenberg, U. Nieken, C. Schwede, C. Zander, *Macromol. React. Eng.* **2019**, *13*, 1900021.
- [10] P. D. Iedema, S. Grcev, H. C. J. Hoefsloot, *Macromolecules* **2003**, *36*, 458.
- [11] P. Pladis, C. Kiparissides, *Chem. Eng. Sci.* **1998**, *53*, 3315.
- [12] R. A. Hutchinson, *Macromol. Theory Simul.* **2001**, *10*, 144.
- [13] P. D. Iedema, M. Wulkow, H. C. J. Hoefsloot, *Macromolecules* **2000**, *33*, 7173.
- [14] K.-D. Hungenberg, M. Wulkow, *Modeling and Simulation in Polymer Reaction Engineering*, Wiley-VCH Verlag GmbH & Co. KGaA, Weinheim, Germany **2018**.
- [15] T. Meyer, J. T. F. Keurentjes, *Handbook of Polymer Reaction Engineering*, Wiley-VCH Verlag GmbH, Weinheim, Germany **2008**.
- [16] M. Wulkow, *Macromol. React. Eng.* **2008**, *2*, 461.
- [17] I. M. Neuhaus, Dissertation, *Technische Universität Darmstadt* **2014**.
- [18] D. Eckes, Dissertation, *Technische Universität Darmstadt* **2017**.